# Dalton Transactions

Accepted Manuscript






ROYAL SOCIETY OF CHEMISTRY

www.rsc.org/dalton

## Graphical Abstract

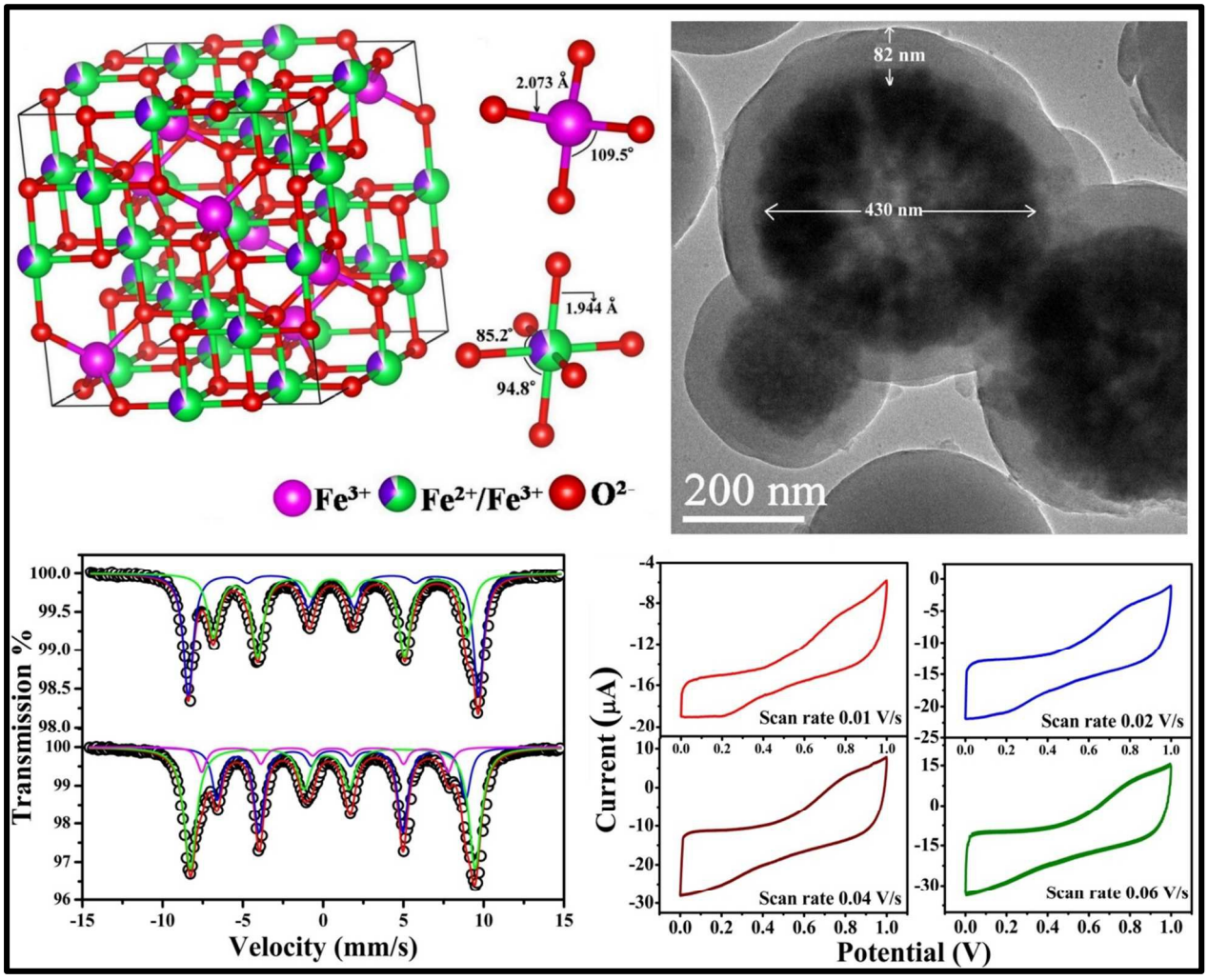


The magnetic and hyperfine properties of $Fe_3O_4$ and $Fe_3O_4@SiO_2$ microspheres depend on synthesis procedure, morphology, surface property, the collective properties of the nanoparticle assembly and the average size of individual nanoparticle forming the spherical ensemble, but not on the diameter of the microspheres. $Fe_3O_4@SiO_2$ can be used for fabrication of electrical double layer capacitor.

# A comparative study on structural, optical and magnetic properties of $Fe_3O_4$ and $Fe_3O_4$@$SiO_2$ core-shell microspheres along with assessment of their potentiality as electrochemical double layer capacitor

S. Majumder,[a, b] S. Dey,[a] K. Bagani,[b] S. K. Dey,[a] S. Banerjee[b,*] and S. Kumar[a,*]

[a] Department of Physics, Jadavpur University, Kolkata – 700032, India

[b] Saha Institute of Nuclear Physics , 1/AF Bidhannagar, Kolkata – 700064, India

**Abstract:**

Herein, we report a comprehensive and comparative study on the crystal structure, microstructural, optical, magnetic, hyperfine and electrochemical properties of $Fe_3O_4$ microspheres (S1) of diameter ~ 418 nm and $Fe_3O_4$@$SiO_2$ core-shell microspheres (S2) of diameter ~ 570 nm. Each asymmetric unit of the crystalline $Fe_3O_4$ has one cation vacancy at octahedral [B] site. At 300 K the saturation magnetization and coercivity of ferrimagnetically ordered S1 and S2 are 63.5, 38.5 emu $g^{-1}$ and 200 and 120 Oe, respectively. We have shown that the synthesis procedure, morphology, surface property, interparticle interaction manifesting the collective properties of the nanoparticle assembly and the average size of individual $Fe_3O_4$ nanoparticles forming the spherical ensemble play the crucial role in determining the magnetic properties of $Fe_3O_4$ and $Fe_3O_4$@$SiO_2$ microspheres while the diameter of the microsphere does not have significant influence on magnetic properties of such system. Further, the photoluminescence intensity of $Fe_3O_4$ microspheres gets significantly enhanced upon $SiO_2$ coating. The cyclic voltammetric study suggests that S1 can act as a good electrical double layer capacitor (EDLC) above the scan rate of 0.04 V/s while S2 exhibits excellent performance as

EDLC in the scan range from 0.01 to 0.06 V/s. Thus, S2 is a potential candidate for fabrication of EDLCs.

**Keywords:**

$Fe_3O_4$ and $Fe_3O_4@SiO_2$ microsphere, electrochemical double layer capacitor, Magnetic property, Mössbauer spectroscopic study, Rietveld refinement, Optical property.

* Corresponding author. E-mail: kumars@phys.jdvu.ac.in, Phone No.: +91-98311-15427

sangam.banerjee@saha.ac.in, Phone No.:+91-9432-671560

## Introduction

In the past decade, a great deal of attention has been paid on the synthesis and study of physical properties of various morphological forms of $Fe_3O_4$ nano and microstructures, like nanoparticles,[1] nanowires,[2] nanotubes,[3] nanocubes,[4] microspheres,[5] hollow microspheres,[6] core-shell nano[7] and microspheres[8] owing to their potential applications in high density storage devices, magnetic sensors, magnetic resonance imaging, magnetically assisted drug delivery, biomaterial diagnostics etc.[1-6,8-13] Among the various morphological forms, the $Fe_3O_4$ microspheres exhibit morphology dependent unique physical properties which are drastically different from those of the constituent $Fe_3O_4$ nanoparticles.[14-17]

Recently, several research groups have proposed that the core-shell micro and nano structures of different materials can be suitably used in diverse technological applications for their multifunctionalities.[18-21] It is noteworthy that in most of the cases, $SiO_2$ has been selected as the shell material mainly due to its biocompatibility and protection effects.[19] The $SiO_2$ coated nanoparticles have been substantially used in biological research because the $SiO_2$ shell obstructs diffusion of chemicals between the inside and outside of the nanoparticles and thus lowers the lethal effect of nanoparticles towards biological cells and tissues.[19] Moreover, owing to its rich surface chemical properties, the $SiO_2$ shell is used for bioconjugation and this has great importance in the field of biomedicine. On the other hand, some of the research groups have developed $SiO_2$ coated quantum dots with improved chemical and photochemical stabilities. Zhang et al. have found that ZnO@$SiO_2$ nanoparticles exhibit striking fluorescence stability in vitro, which can be suitably used in diverse biomedical applications.[19] It has been reported that the intrinsic properties (magnetic and dielectric properties) of bulk $BiFeO_3$ particles can be enhanced by encapsulating them with $SiO_2$ shell.[18] Further the Au@$SiO_2$ and Ag@$SiO_2$ core-

shell nanoparticles have been successfully studied to get functional materials with enhanced optical properties.[20, 21]

Apart from these, the core-shell microstructures comprising of magnetic core and nonmagnetic shell have recently emerged as an attractive area of research mainly because of their bifunctionalities.[14,15] In this regard, the $Fe_3O_4$ microspheres coated with $SiO_2$ shell ($Fe_3O_4$@$SiO_2$) are extensively investigated due to their spherical shape, smooth surface, large surface area, high saturation magnetization, low toxicity, good dispersion in liquid medium and good stability and these endow them with wide range of application possibilities in biomedical field.[14,15,22] It is well known that $Fe_3O_4$ nanoparticles below 11.5 nm in size exhibit superparamagnetic behavior[23,24] and it is very difficult to retain the assembled structure of superparamagnetic particles without application of magnetic field. Up till now, the major emphasis is therefore devoted to the synthesis of $Fe_3O_4$ microspheres and core-shell $Fe_3O_4$ microspheres.[14-17,22] Generally, $Fe_3O_4$ microspheres are prepared by assembling $Fe_3O_4$ nanoparticles using organic surfactant. It is noteworthy that polyethylene glycol is considered as efficient capping and interaction reducing agent. This has been successfully used to capture a large number of $Fe_3O_4$ nanoparticles to form the stable $Fe_3O_4$ microspheres.[15]

The $Fe_3O_4$ microsphere is treated as self assembly of discrete $Fe_3O_4$ nanoparticles[25] but it always exhibits higher saturation magnetization compared to its discrete nanoparticle building blocks. According to the literature, usually $Fe_3O_4$ microspheres of size ranging between 200-400 nm built up with nanoparticles below 20 nm exhibit high saturation magnetization ($M_{SAT}$) and low coercivity ($H_C$) at room temperature and these are very useful for biomedical applications.[5,6,22] At room temperature, the $M_{SAT}$ and $H_C$ of the hierarchical hollow microsphere of size 200-300 nm built up with nanoparticles having diameter 20-30 nm are 81.4 emu $g^{-1}$ and

34.1 Oe, respectively,[6] whereas the $M_{SAT}$ and $H_C$ of $Fe_3O_4$ nanoparticle building blocks with diameter 20 nm are 77.2 emu $g^{-1}$ and 27.7 Oe, respectively. It is noteworthy that among various morphological forms of $Fe_3O_4$ microspheres, the single crystalline hollow microspheres of diameter 200 nm show the highest $M_{SAT}$ (~81.9 $emug^{-1}$) [5] and $H_C$ (~94 Oe) at 300 K.[26]

Usually, with the incorporation of nonmagnetic $SiO_2$ shell over $Fe_3O_4$ microspheres, the magnetization of the resultant $Fe_3O_4$@$SiO_2$ microspheres reduces due to lower $Fe_3O_4$ mass fraction in the core-shell system, formation of a magnetic dead layer at the interface between $Fe_3O_4$ microsphere and $SiO_2$ shell and the spin canting effect. For example, at 300 K, the $M_{SAT}$ of $Fe_3O_4$@$SiO_2$ microspheres obtained by coating $SiO_2$ layer of thickness 70 nm on $Fe_3O_4$ microspheres of diameter 300 nm having $M_{SAT}$ 80.7 emu $g^{-1}$ is 68.2 emu $g^{-1}$.[16] At 300 K, the $M_{SAT}$ (53.3 emu $g^{-1}$) of mesoporous silica coated superparamagnetic $Fe_3O_4$@$SiO_2$ microspheres sandwich structure (500 nm) is much less than that of $Fe_3O_4$ ($M_{SAT}$ = 80.7 emu $g^{-1}$) and $Fe_3O_4$@$SiO_2$ microspheres.[14] At 300 K, the values of $M_{SAT}$ and $H_C$ of $Fe_3O_4$@$SiO_2$ microspheres having core diameter of 570 nm and shell thickness of ~ 100 nm prepared by modified Stöber sol-gel process are less than those of $Fe_3O_4$ microspheres.[22] On the other hand, for $Fe_3O_4$@$SiO_2$ microspheres, synthesized by hydrolysis and condensation technique, the value of $M_{SAT}$ decreases and that of $H_C$ increases with the increase in $SiO_2$ shell thickness.[15]

In the literature, there are several reports on the study of both low and room temperature magnetic properties of $Fe_3O_4$ nanoparticles and $Fe_3O_4$-$SiO_2$ nanocomposites.[26] On the other hand, although the magnetic properties of $Fe_3O_4$ and $Fe_3O_4$@$SiO_2$ microspheres have been widely investigated at room temperature (~ 300 K), no report is available on the low temperature magnetic properties of $Fe_3O_4$ and $Fe_3O_4$@$SiO_2$ microspheres. Given this where the study on magnetic properties of $Fe_3O_4$ and $Fe_3O_4$@$SiO_2$ microspheres stands now, a comparative study on

the low temperature magnetic properties of $Fe_3O_4$ and $Fe_3O_4$@$SiO_2$ microspheres appears to be essential for the better understanding of their magnetic properties. Further, according to the earlier reports, the structure and morphology play the decisive role in determining the magnetic properties of both $Fe_3O_4$ and $Fe_3O_4$@$SiO_2$ microspheres.[5,6,14,16] However, to the best of our knowledge, even the crystal structures of $Fe_3O_4$ and $Fe_3O_4$@$SiO_2$ have not been reported. Additionally, the deviation from exact stoichiometry is an inherent feature of $Fe_3O_4$ nanostructures. The Mössbauer spectrometry is regarded as the most reliable technique to evaluate the exact stoichiometry as well as to probe the superparamagnetic behavior of such systems. It has not yet been applied to find the correct stoichiometry and evaluate the hyperfine properties of $Fe_3O_4$ and $Fe_3O_4$@$SiO_2$ microspheres. There are also some reports on the electrochemical properties of different morphological forms of nanostructued $Fe_3O_4$ but no such report is available for $Fe_3O_4$ and $Fe_3O_4$@$SiO_2$ microspheres. In this background, our aim is to study the structural, microstructural, optical, low temperature magnetic, hyperfine and electrochemical properties of $Fe_3O_4$ microspheres (S1) and $Fe_3O_4$@$SiO_2$ microspheres (S2) and to compare these properties of S1 vis-á-vis those of S2.

## Experimental

### Synthesis of $Fe_3O_4$ microspheres

All the chemicals used (ferric chloride hexahydrate ($FeCl_3.6H_2O$), polyethylene glycol (PEG), sodium acetate trihydrate ($CH_3COONa.3H_2O$), ethylene glycol ($CH_3CH_2OH$), ammonium hydroxide ($NH_3.H_2O$, 25%), ethanol ($C_2H_5OH$) and tetraethyl orthosilicate (TEOS)) were purchased from Merck-India Pvt. Ltd. and were used without further purification. The $Fe_3O_4$ microspheres have been synthesized by solvothermal method. At first, 2.025 gm

$FeCl_3.6H_2O$, 1.500 gm PEG ($M_w$ = 4000) and 5.400 gm $CH_3COONa.3H_2O$ were dissolved in 60 ml ethylene glycol. The mixture was stirred vigorously for 30 minutes and a yellowish solution was obtained. The mixture was then transferred into a 100 ml Teflon-lined stainless steel autoclave and heated at 180 ºC for 20 hours in a muffle furnace. Thereafter the furnace was allowed to cool down to room temperature at a cooling rate of 3 ºC $min^{-1}$. A black product was formed and it was collected by magnetic separation technique. The sample was then washed several times with deionized water and ethanol. Finally, the specimen was collected by ultracentrifugation and dried at 60 ºC for 6 hours in vacuum and the $Fe_3O_4$ microspheres (S1) were obtained.

**Synthesis of $Fe_3O_4$@$SiO_2$ microspheres**

The $Fe_3O_4$@$SiO_2$ core-shell microspheres were prepared by modified Stöber sol-gel method. Firstly, 400 mg of S1 was dispersed in water-ethanol solution (1:5 volume ratio) by ultrasonication for 30 minutes. Subsequently, another solution of $NH_3$ (25%) and tetraethyl orthosilicate (TEOS) in 1.0:0.8 volume ratio was prepared separately. These two solutions were mixed together and vigorously stirred for 3 hours. The resultant product was magnetically separated and washed with deionized water and ethanol. Finally, the precursor was collected by centrifugation and dried at 60 ºC in vacuum for six hours and the $Fe_3O_4$@$SiO_2$ core-shell microspheres (S2) were obtained.

**Characterization techniques**

The samples are characterized by powder X-ray diffraction (PXRD), field emission scanning electron microscopic (FESEM), energy dispersive X-ray spectroscopic (EDS), high resolution transmission electron microscopic (HRTEM), Fourier transform infrared spectroscopic (FTIR), UV-Vis and Raman spectroscopic techniques. The PXRD pattern of the

sample has been recorded by Bruker D8 Advanced Diffractometer using Cu Kα (λ = 1.54184 Å) radiation. The generator was set at 40 kV and 40 mA. The diffraction patterns were recorded at room temperature (21° C) with step size of 0.0199° and a counting time of 5 s/step over the range of 2θ = 15° - 80°. The FESEM (FEI, INSPECT F50) was used for the morphological and microstructural characterizations. The chemical compositions of the samples were determined by BRUKER EDS system attached with the FESEM equipment. The HRTEM micrographs of S1 and S2 have been recorded by JEOL, 2100 HRTEM. The FTIR spectra of the samples have been recorded by Perkin Elmer Spectrum Two FTIR spectrometer. The UV-Vis spectral data of S1 and S2 are collected by dispersing them in distilled water through vigorous ultrasonication using JASCO V-630 spectrophotometer within the wavelength range of 240 – 450 nm. The photoluminescence (PL) spectra of S1 and S2 have been recorded by JASCO FP-6700 spectrophotometer in the wavelength range of 400 - 500 nm. The Raman spectra of S1 and S2 have been recorded by WITEC alpha, 300R instrument equipped with diode laser source of λ= 532 nm for further investigation of the influence of $SiO_2$ coating on the $Fe_3O_4$ micropspheres. To get Raman spectra with lower noise profile, thin film of the sample over glass slide has been used instead of powder sample. The film was developed by drop cast technique.

The dc magnetization (M) as a function of temperature (T) and magnetic field (H) was measured using physical property measurement system (PPMS, Quantum Design). The M(T) data were recorded under zero field cooled (ZFC) and field cooled (FC) modes. In ZFC mode of measurement, the sample was cooled from 310 K to 5 K in absence of dc magnetic field while in the FC mode, the sample was cooled in presence of 100 Oe external magnetic field. The M(T) data were recorded in the presence of measurement field in the heating cycle. The data for magnetic field dependence of magnetization (hysteresis loops) were recorded at 5, 100 and 300

K in the ZFC mode. The room temperature Mössbauer spectra of the samples were recorded in transmission geometry using constant acceleration drive (CMTE-250) with a 20 mCi $^{57}Co$ source in Rh matrix. The electrochemical properties of the ITO-S1 and ITO-S2 (ITO: Indium-tin-oxide) electrodes were studied by cyclic voltammetry (CV) using CHI 660C electrochemical workstation. The ITO-S1 electrode has been developed using the following procedure. At first, 10 mg of sample (S1/S2) was dispersed in 10 mL distilled water by vigorous ultrasonication. Then the dispersion was poured dropwise onto an ITO coated glass slide placed on the platform of a spin coating unit (SCU-2007). A uniform thin film of the sample was deposited on ITO coated glass slide by spin coating for 5 minutes at 1500 rpm. Finally, the film was heated under vacuum at 120$^{\circ}$ C for 30 minutes to evaporate the solvent (water) from the deposited film. We have used a three electrode system with ITO-S1 or ITO-S2 electrodes as cathode, Pt wire as anode and Ag/AgCl solution as reference electrode. 1M aqueous solution of $Na_2SO_4$ was used as electrolyte due to its high ionic conductivity, low cost and non-flammability.

## Result and discussion

### Powder X-Ray Diffraction (PXRD) study

We have indexed the PXRD patterns of S1 and S2 by DICVOL06 and TREOR90 of Fullprof.2k package.[28,29] The statistical analysis of PXRD data has been performed by FINDSPACE of EXPO2009 package to determine the space group of the samples.[30] The preliminary structural analysis indicates that only the characteristic diffraction peaks for spinel ferrite phase are present in the PXRD pattern of S1 and S2. The Miller indices and the space group obtained for S1 are in good agreement with JCPDS database (JCPDS No.85-1436).[6] This indicates that S1 is a single phase well crystalline spinel ferrite. At this stage, our aim of structural analysis is to recognize the changes in crystal structure of S1 due to $SiO_2$ coating by

comparing the crystal structure of S1 and S2. So, while calculating the theoretical PXRD pattern of S2 through Rietveld refinement of the PXRD data, we have not considered the amorphous hump region of the experimentally obtained PXRD pattern of the sample.

It may be noted that the Rietveld refinement method is a well established tool for structural and microstructural characterization of powder sample.[31-34] We have performed the Rietveld refinement of the PXRD data to determine the structural (atomic coordinates, lattice parameters) and microstructural (crystallite size, microstarin) parameters. The structural and microstructural refinements have been carried out by the Rietveld based software package MAUD2.33 since this package can successfully extract the structural and microstructural (crystalline sizes, r.m.s strain) parameters simultaneously.[35] At the beginning, all the necessary structural information and some starting values of microstructural parameters have been provided. For $Fe_3O_4$ phase, the initial positions of tetrahedral (A) site metal ions, octahedral [B] site metal ions and O ions have been assigned in the special Wyckoff positions 8b (0.125, 0.125, 0.125), 16c (0.5, 0.5, 0.5) and 32e (0.258, 0.258, 0.258), respectively. The occupancies of the iron ions were set at the values in accordance with those obtained from Mössbauer spectroscopic study. After a few successful refinement cycles, we have obtained the refined lattice parameters, crystallite size and r.m.s strain with satisfactory values of $R_{wp}$, $R_{exp}$ and GOF (Table 1). The results are illustrated in Fig. S1. The relevant microstructural parameters are summarized in Table 1.

The Rietveld refinement of PXRD data has also been carried out using GSAS[36] program with EXPGUI[37] interface to determine the crystal structure more precisely. The results are presented in Figs. 1 and S2. The statistical and Rietveld analysis of PXRD patterns have together with revealed that both S1 and S2 have been crystallized in $Fd\bar{3}m$ space group with cubic

symmetry and the relative occupancies of $Fe^{3+}$ at tetrahedral (A) site, $Fe^{2+}$ at octahedral [B] site, $Fe^{3+}$ at [B]-site and $O^{2-}$ ions are 1, 0.625, 0.3125 and 1, respectively. The asymmetric unit of both compounds contains 23 iron ions (8 $Fe^{3+}$ ions at (A) sites, 10 $Fe^{2+}$ at [B] sites and 5 $Fe^{3+}$ ions at [B] sites) and 32 oxygen ions. In general, the cubic spinel ferrites have 24 metal ions (8 at (A) sites and 16 at [B] sites) in each asymmetric unit. Thus, for both S1 and S2 there exists one iron ion vacancy at octahedral [B] site. The results of Rietveld analysis indicate that the unit cell volume and crystallite size of S2 is less than those of S1 whereas the microstrain of S2 is greater than that of S1. Thus the results suggest that the lattice gets contracted and microstrain enhances upon $SiO_2$ coating on $Fe_3O_4$ microspheres. The $(Fe\text{-}O)_A$ bond lengths for S1 and S2 are 2.073(7) and 2.0455(1), respectively, and $(Fe\text{-}O)_B$ bond lengths of S1 and S2 are 1.944(7) Å and 1.9001(1) Å, respectively. This small difference between the bond lengths of S1 and S2 is due to slight mismatch between the coordinates of their oxygen ions (Fig. 2). The final crystallographic and refinement parameters, bond lengths and bond angles are listed in Table 2.

**FESEM study**

The FESEM micrographs of S1 and S2 are presented in the Fig. 3 and Fig. 4. In the SEM images of S1, the sub-microspheres with average diameter of about 415 nm formed by the self-assembly of nanometric $Fe_3O_4$ have been clearly observed (Fig 3). The surfaces of such spheres appear to be slightly rough. Unlike S1, a large variation of contrast has been observed in the SEM image of the microspheres of S2. This variation of contrast in the core and shell regions of the microspheres belonging to S2 has enabled us to distinguish between the core and shell regions and to determine the core diameter and shell thickness. The central black region having average diameter ~ 418 nm and the outer gray part with average thickness ~ 75 nm of each microsphere can be assigned to crystalline $Fe_3O_4$ core and amorphous $SiO_2$ shell, respectively.

The average diameter of $Fe_3O_4$@$SiO_2$ is ~ 570 nm. Moreover, it has been noticed that the surfaces of the microspheres of S2 is smoother than that of S1. This implies that the roughness of the surface of $Fe_3O_4$ microspheres get wiped out upon $SiO_2$ coating on them. The SEM image of the sample S2 confirms the deposition of $SiO_2$ layer at the surface of $Fe_3O_4$ sub-microspheres. The EDS spectra of S1 and S2 showing the peaks for the constituent elements are illustrated in Fig. 3 (d) and 4 (d).

**HRTEM study**

To crosscheck the results of PXRD and FESEM study and to gather more detailed structural and microstructural information, we have carried out the HRTEM analysis of the samples. The TEM micrographs at low and high magnification of S1 and S2 along with the selected area electron diffraction (SAED) pattern of S1 have been shown in the Fig. 5 and Fig. 6. The HRTEM images of S1 indicate that the average diameter of $Fe_3O_4$ microspheres is ~ 418 nm. A close inspection of microspheres revealed that it has been formed by the self assembly of $Fe_3O_4$ nanoparticles of average size ~18.5 nm. The well defined lattice fringes and prominent rings in the SAED image suggest that the sample is well crystalline in nature. The observed crystallographic "d" values match well with those obtained from the PXRD study [Fig. 5(d)].

The HRTEM image of S2 confirms the formation of $SiO_2$ shell over the surface of the $Fe_3O_4$ core. The diameter of the core region is ~ 418 nm and the thickness of the shell region varies from 50–125 nm. In case of S2, due to amorphous $SiO_2$ coating over the $Fe_3O_4$ microspheres, the individual nanoparticles inside the core region are not observed distinctly.

**FTIR study**

To characterize the samples and to probe the presence of any impurity phase we have recorded the FTIR spectra of S1 and S2 in solid state using KBr matrix (Fig. 7). For both S1 and

S2 a strong peak at 567 $cm^{-1}$ along with a shoulder at 618 $cm^{-1}$ are observed due to the stretching vibrational mode of the Fe-O functional group of $Fe_3O_4$[13,38] and the broad band centered around 3400 $cm^{-1}$ can be assigned to stretching vibration of O-H of the free or absorbed water molecules. The strong asymmetric stretching vibration of Si-O-Si at 1080 $cm^{-1}$, symmetric vibration of Si-O-Si at 798 $cm^{-1}$ and the symmetric stretching vibration of Si-OH bond at 960 $cm^{-1}$ are observed in the FTIR spectrum of S2.[13] Again, sharp band around 574 $cm^{-1}$ corresponds to Si-O-Fe stretching vibration.[39]

**Raman spectroscopic study**

The Raman spectroscopy is an efficient tool in the field of material science to identify different phases present in the sample. The room temperature Raman spectra of S1 and S2 are presented in Fig. 8. For $Fe_3O_4$ microspheres, an intense peak has been noticed at ~ 678 $cm^{-1}$ and this may be attributed to $A_{1g}$ mode of symmetric stretch of oxygen atoms along the Fe–O bonds.[40] The other two weak peaks at about 300 and 545 $cm^{-1}$ are assigned to the $T_{2g,3}$ and $T_{2g,2}$ vibration modes of $Fe_3O_4$, respectively.[41,42,43] The Raman spectrum of S2 shows the presence of additional peaks along with the peaks due to $Fe_3O_4$ phase. The peaks at about 480, 365 and 216 $cm^{-1}$ confirm the presence of $SiO_2$ in S2. In the sample S2, the presence of characteristic Raman peaks of $SiO_2$ along with the subsequent decrease in intensity and slight positional shift of $Fe_3O_4$ Raman peaks in S2 compared to S1 give the evidence in favor of the formation of $Fe_3O_4$@$SiO_2$ core-shell structure formation for S2.[44] It may be noted that the characteristic Raman peaks of $SiO_2$ slightly changes when $Fe_3O_4$@$SiO_2$ core-shell structure formation takes place. The broadening of the $SiO_2$ peak at ~ 365 $cm^{-1}$ may be due to the vibration mode corresponding to the Fe-O-Si bond present in the boundary region of $Fe_3O_4$@$SiO_2$ microsphere.[45] The formation of FeOOH, α-$Fe_2O_3$ and γ-$Fe_2O_3$ as impurity in the sample can be easily confirmed by

identifying their peaks at higher wave number (in the range of 1300-1400 $cm^{-1}$).[42,43] In the present case, we have not observed any peak in higher wave number region. So, it may be confirmed that the $Fe_3O_4$ present in S1 and S2 are pure in nature.

The presence of Si-O-Si, Fe-O-Si/ Si-O-Fe and Si–OH bonds in the FTIR spectra and the core shell morphology of S2 as revealed by SEM and Raman spectroscopic study can be accounted by the scheme depicted in Fig. 9. It may be noted that such scheme was proposed by Du et al for $Fe_3O_4$@$SiO_2$ core-shell nanoparticles.[39]

**Optical study**

The UV-Vis spectra of S1 and S2 are illustrated in Fig. 10. A large hump has been noticed in between 320-390 nm in the UV-Vis absorption spectrum of S1, which is in well agreement with the earlier reported results.[46] On the other hand, S2 exhibits a peak at about 269 nm and a hump in between 320-390 nm. Comparing the UV-Vis spectrum of S2 with that of S1, it is clear that the hump in between 320-380 nm in case of S2 is due to the presence of $Fe_3O_4$ and the peak at about 269 nm may be attributed to $SiO_2$. Moreover, the lowering of intensity in the optical absorption of $Fe_3O_4$ in S2 with respect to S1 is due to the presence of $SiO_2$ in S2.

The photoluminescence (PL) emission spectra of the samples S1 and S2 at an excitation wavelength of 360 nm are presented in Fig. 11. It is evident from the result that the sample S2 exhibits enhancement in the luminous intensity compared to that of S1 without any appreciable shift in the peak position. According to the SEM study, the encapsulation of $Fe_3O_4$ microsphere with $SiO_2$ layer reduces surface defects and therefore the number of trap states in the system decreases and this in turn reduces indirect transitions through trapped states and the majority of electrons relax through direct transition between conduction and valence bands. Such direct

transition is the possible cause for enhancement of the photoluminescence intensity of S2 compared to S1.

**Mössbauer Spectroscopic study**

The $^{57}$Fe Mössbauer spectroscopy is an efficient tool to probe the nature of magnetic ordering of iron containing materials.[31-34] To determine the nature of magnetic order in S1 and S2 we have fitted the Mössbauer spectra of the samples with Lorentzian profile using the Recoil program.[47] The results are presented in Fig. 12 and the hyperfine parameters are listed in Table 3. It is clear from the IS values that both $Fe^{2+}$ and $Fe^{3+}$ ions are present in the samples.[48,49] For $Fe_3O_4$, due to continuous electron hopping between $Fe^{2+}$ and $Fe^{3+}$ ions in the [B] site, the nuclei feel an average valence (mixed valence) of $Fe^{2.5+}$ in the [B] site. In case of $Fe_3O_4$ nanostructures, the introduction of vacancies at the [B] site during the reaction procedure results in the formation of nonstoichiometric iron oxide with the formula $(Fe^{3+})_A [Fe_{(1-3x)}{}^{2+} Fe_{(1+2x)}{}^{3+}\Phi_x]_B O_4$, where $\Phi$ represents the [B] site vacancy. Now, if $RA_B$ and $RA_A$ are the relative areas of (A) and [B] site sextets then we can write $RA_B / RA_A = (2 – 6x) / (1+ 5x)$.

We have fitted the Mössbauer spectrum of S1 with two different sextets accounting for iron ions at the (A) and [B] sites. Generally, for $Fe_3O_4$ the sextet with lower isomer shift (IS) value and higher hyperfine field is assigned to $Fe^{3+}$ ions at (A) site and the other sextet with higher IS value and lower hyperfine field is attributed to iron ions at [B] site. From the area under (A) and [B] site sextets we have calculated the cation distribution and [B] site vacancy for S1 using the above formula and the result indicates that the stoichiometry of S1 is $(Fe^{3+}) [Fe_{0.675}{}^{2+} Fe_{1.215}{}^{3+} \Phi_{0.1075}]O^{2+}{}_4$.

The Mössbauer spectrum of S2 can be best fitted with three sextets. Among these three sextets two are attributed to iron ions at (A) and [B] sites and the third component (~11%)

having lower value of hyperfine magnetic field originates from the interfacial region between $Fe_3O_4$ core and $SiO_2$ shell of S2. The lower value of hyperfine field of the third component may be due to spin canting effect at the interface between $Fe_3O_4$ core and $SiO_2$ shell. It is well known that the IS of Mössbauer spectrum depends on chemical environment persisting around the iron ion. The chemical environment also determines the nature and number of subpattern in the Mössbauer spectrum of a sample. The change in IS values of (A) and [B] subspectra of S1 and S2 and the appearance of a third component in spectrum of S2 indicate that the chemical environment around some iron ions has significantly changed upon $SiO_2$ coating on S1 due to chemical bonding between atoms of the core and the shell. This gives further evidence in favor of the formation of Fe-O-Si, Si-O-Fe bonds as revealed by FTIR study.

We have evaluated the [B] site cation vacancy of S2 following the same method used for S1 and obtained the stoichiometric formula of S2 as $(Fe^{3+})$ $[Fe_{0.842}^{2+}\ Fe_{1.105}^{3+}\ \Phi_{0.0525}]O_4$. The lowering of hyperfine field in S2 compared to S1 implies the reduction of magnetization in S2 with respect to S1. The increase in line width along with the reduction of hyperfine field in case of S2 compared to S1 suggests that the encapsulation of S1 with $SiO_2$ introduces the relaxation and this is due to reduction of anisotropy energy of S2 compared to S1.

**Magnetic study**

A straightforward and rapid estimation of the blocking temperature can be done by using the zero field cooled (ZFC) and the field cooled (FC) protocol experiments. The ZFC curve of superparamagnetic nanoparticles exhibits maxima at blocking temperature ($T_B$) and the FC curve coincides with the ZFC curve at the temperature of irreversibility ($T_{irr}$), which is related to the blocking of largest particles.[31,32] The ZFC and FC magnetizations of S1 and S2 have been recorded at 100 Oe external magnetic field in the temperature range 5–300 K (Fig. 13). For both

S1 and S2 the ZFC magnetization decreases monotonically and the FC magnetization remains almost constant with the lowering of temperature. So, it may be inferred that the samples exhibit magnetically well ordered state within the measurement temperature range and the blocking temperature ($T_B$) is well above the range of measurement temperatures. No signature of the Verwey transition has been noticed in the ZFC magnetization curves of S1 and S2. It is well known that the Verwey transition temperature shifts toward lower temperature with decrease of particle size and it no longer remains observable for particles having size below 11.5 nm.[23] Here the Verwey transition has not been observed in S1 and S2 as these microspheres are formed by self-assembly of very small particles (average particle size ~ 18 nm). On the other hand, the $Fe_3O_4$ nanoparticles having size below 20 nm usually exhibit superparamagnetic behavior at room temperature[22,24] whereas the Mössbauer spectroscopic study and the ZFC-FC measurements together suggest that both S1 and S2 are in ferrimagnetic state at room temperature. It is noteworthy that $T_B$ of $Fe_3O_4$ nanoparticles having size ~ 17.9 nm is 220 K while the blocking temperatures of both S1 and S2 are above 300 K, although they are built up with nanoparticles of average size ~ 18.5 nm. Here the blocking temperatures of S1 and S2 have shifted toward higher temperature with respect to the constituent nanosized building blocks due to very strong interparticle interaction. Such shifting of $T_B$ with interparticle interaction has been discussed in the literature.[31,32] It may further be noted that, according to the TEM study $Fe_3O_4$ nanoparticles get strongly agglomerated after encapsulation of $Fe_3O_4$ nanoparticles with $SiO_2$ shell. This is expected to enhance the $T_B$ of S2 with respect to S1. It is clear from the ZFC-FC magnetization study that in both the cases the $T_B$ is higher than 300 K, which is the highest accessible measurement temperature for our instrument. Therefore, the role of such aggregation could not be quantitatively assessed in the present case.

The disappearance of Verwey transition in the ZFC curve of S1 and S2 suggests that the $Fe_3O_4$ nanoparticles of $Fe_3O_4$ microsphere and $Fe_3O_4$@$SiO_2$ microsphere retain their individual magnetic property while the collective behavior of $Fe_3O_4$ nanoparticles forming the microspheres is manifested by the shift of the blocking temperatures of S1 and S2 toward higher temperature with respect to their constituent magnetic nanoparticles. The field dependence of magnetization (*M–H* loop) of S1 and S2 has been recorded at 300, 100 and 5 K in the field range of -5 to +5 T and are depicted in Fig. 14. It is clear from the results of M–H measurements that the samples exhibit clear hysteresis loops at all of these temperatures. The ZFC and FC magnetizations and M-H measurements indicate that the samples are in magnetically ordered state between 300–5 K. The saturation magnetization ($M_{SAT}$) of the samples is calculated from the *M* vs. *1/H* plot using the law of approach to saturation. The values of $M_{SAT}$ and coercivity ($H_C$) of the samples are listed in Table 4.

The values of $M_{SAT}$ of $Fe_3O_4$ hierarchical sub-microspheres having diameters of 200–300 nm built up with nanoparticles of diameters ranging between 20–30 nm synthesized by solvothermal method,[6] single crystalline microspheres with diameter of 200 nm synthesized by solvothermal method,[5] single crystalline hollow sub-microspheres having diameter ranging between 200-300 nm,[26] solid microspheres of diameter 400 nm built from nanoparticles of size 20 nm prepared by hydrothermal method,[15] the $Fe_3O_4$ microsphere having diameter 300 nm built up with nanoparticles of diameter 30 nm[16], spherical nanoporous microspheres of $Fe_3O_4$ having diameter 100 nm built up with nanoparticles of size 5 nm[25] and S1 at 300 K are 81.4, 81.9, 68 , 82, 80.7, 42.8 and 63.5 emu $g^{-1}$, respectively. Again, the coercitivity ($H_C$) of $Fe_3O_4$ hierarchical sub-microspheres having diameters of 200–300 nm built up from nanoparticles with diameters 20-30 nm synthesized by solvothermal method,[6] single crystalline hollow sub-microspheres

having diameter ranging between 200-300 nm,[26] solid microspheres of diameter 400 nm built up from nanoparticles of size 20 nm prepared by hydrothermal method[15] and spherical nanoporous microspheres of $Fe_3O_4$ having diameter 100 nm built up with nanoparticles of size 5 nm[25] at 300 K are 34.1, 94, 100 and 44 Oe, respectively, while the $H_C$ of S1 is 200 Oe. Hence, the present work strongly corroborates the earlier results that in general $Fe_3O_4$ microspheres exhibit high saturation magnetization and low coercitivity at room temperature. It further indicates that both the saturation magnetization and coercitivity of $Fe_3O_4$ microspheres increase with the decrease of temperature, due to blocking of constituent magnetic nanoperticles of the microspheres. However, it has also been reported that $Fe_3O_4$ microspheres having diameter 300 nm consisting of nanoparticles of diameter 15 [14] and 30 nm[16] exhibit superparamagnetic behavior (do not show any hysteresis loop) at 300 K. The present study however does not support these findings. Moreover, Cheng et al.[15] have reported that the $M_{SAT}$ and $Hc$ of $Fe_3O_4$ microspheres of diameter ranging between 200-600 nm built from nanoparticles of size 20 nm is ~ 82 emu $g^{-1}$ and 100 Oe, respectively, irrespective of diameters of the microspheres. Based on the results of previous and present works, it may therefore be inferred that the coercivity and saturation magnetization of $Fe_3O_4$ microspheres strongly depend on the morphology and synthesis procedure but the magnetic properties of $Fe_3O_4$ microspheres do not depend upon the diameter of the microsphere and it is mainly determined by the average particle sizes of its constituent nanoparticle building blocks.

In the present case, both $M_{SAT}$ and $H_C$ of S2 have reduced substantially with respect to those of S1. Such decrease of $M_{SAT}$ and $H_C$ of $Fe_3O_4$ microspheres upon $SiO_2$ coating is in agreement with most of the earlier findings.[14,16] It is quite obvious that the encapsulation of $Fe_3O_4$ with nonmagnetic $SiO_2$ layer will definitely reduce the mass fraction of magnetic

component in the resultant specimen and it might promote spin disorder at the interface between the $Fe_3O_4$ microspheres and $SiO_2$ layer, resulting in the reduction of $M_{SAT}$ in $Fe_3O_4$@$SiO_2$ core-shell microspheres compared to $Fe_3O_4$ microspheres. The results of ZFC-FC magnetization and M-H measurements corroborate with each other and have revealed that both the samples exhibit magnetically well ordered state and there is no signature of superparamagnetic relaxation or spin freezing in the measurement temperature range of 5-300 K. Due to its high saturation magnetization, the magnetic response of S1 will be better than that of S2 whereas due to low coercivity, S2 could be more easily dispersed and rapidly redispersed after removal of magnetic field in water or other liquid medium. Hence S1 is suitable for application in sensing and memory devices while S2 can be utilized in biomedical applications.

**Electrochemical Performance study**

The cyclic voltagrams of ITO-S1 and ITO-S2 films at different scan rates in the voltage range of 0-1 V are presented in Fig. 15 (a) and (b). The cyclic voltagrams of ITO-S1 film are distinctly different at high and low scan rates. The CV plot of ITO-S1 at scan rate of 0.01 V/s exhibits clear oxidation peak at 0.38 V with the corresponding reduction peak at 0.14 V. The redox peaks in the CV curve have been observed up to the scan rate of 0.04 V/s. It may be noted that the intensity of the redox peaks decreases gradually and the oxidation peak shifts towards higher potential whereas the reduction peak shifts towards lower potential with the increase of scan rate and ultimately the redox peaks vanish at higher scan rate. These indicate that at slow scan rate the $Fe_3O_4$ microspheres get sufficient chance to interact with the ions of the electrolyte due to slow ionic motion while at higher scan rate the ions in the electrolyte fail to recognize $Fe_3O_4$ nanoparticles in the $Fe_3O_4$ microspheres. Additionally, the results suggest that the surface of the electrode is homogeneously electroactive at a slower scan rate while at higher scan rate the

voltammetry probes the intercalation process in ion insertion.[50,51] However, the CV curves obtained at scan rate above 0.04 V/s are almost rectangular in shape, which can be attributed to the electrochemical double layer capacitive behavior of the ITO-S1 electrode.[52]

No redox peaks have been observed in the CV curves of ITO-S2 films recorded in the voltage range of 0-1 V at different scan rates between 0.01-0.06 V/s. The nearly rectangular shape of these CV curves indicates that ITO-S2 film exhibits nearly ideal electrochemically double layer capacitive behavior. Having rectangular shaped CV over a wide range of potential and scan rate is the ultimate goal of electrochemically double layer capacitors (EDLCs), which have promising application as pulse power source for digital communication device and electric vehicles.[52] The rectangular shape of CV curve implies that high amount of electrical energy can be stored in the EDCLs fabricated by using S2 during charging and for these devices there will be very low loss of energy due to discharging effect.[52] Hence, S2 appears to be very suitable for fabrication of EDLCs with very high energy storage density. It may also be noted that upon $SiO_2$ coating over $Fe_3O_4$ microspheres the redox behavior of $Fe_3O_4$ disappears and it exhibits enhancement in the electrochemical double layer capacitive behavior. Our result also suggests that for S2, the outer $SiO_2$ layer restricts the ions in the electrolyte to interact with nanoparticles of $Fe_3O_4$ microspheres, as a result of which it exhibits nearly ideal electrochemically double layer capacitive behavior.

It is evident from the literature survey that various morphological forms of $Fe_3O_4$ and $Fe_3O_4@SiO_2$ nano and microstructures (like microspheres, nanocomposite, nanoparticle, nanosheets etc.) can be profitably used in diverse technological applications.[53,54] The superparamagnetic $Fe_3O_4$ nanoparticles are considered to be a successful magnetic resonance imaging (MRI) contrast agent in biomedical and clinical applications.[53,54] Recently Tian et al.

have shown that the $Fe_3O_4$ nanoparticles coated with $SiO_2$ shell exhibit higher stability in human mesenchymal stem cells, which can be suitably used in safe and efficient stem cell tracking system.[55] The $Fe_3O_4$@$SiO_2$@PMMA (Poly methyl methacrylate) core-shell microspheres undergo good dispersal quality and can be used to fabricate core-shell microspheres with different polymers for bioseparation applications.[56] The $Fe_3O_4$@$SiO_2$@Ag core-shell structure synthesized by ultrasonic route shows satisfactory sensitivity, stability and ample recycling performance in surface enhanced Raman scattering.[57] The $Fe_3O_4$@$SiO_2$ nanoparticles conjugated with $NaYF_4$:Yb, Er shell (i.e., $Fe_3O_4$@$SiO_2$/ $NaYF_4$:Yb, Er) have been successfully developed for magnetic targeting and fluorescence imaging, which combined with $MnO_2$ nanosheet can be used as an elegant magnetically guided drug delivery system.[58] Ammonium molybdate deposited amorphous $Fe_3O_4$@$SiO_2$ core-shell nanocomposite has been effectively used as a catalyst in green and efficient one pot synthesis of 2-benzimidazoles at room temperature.[59] The $Fe_3O_4$@$SiO_2$@Ni-La-B magnetic core shell nanocomposite has been found to exhibit excellent selectivity in catalytic hydrogenation of benzophenone to benzhydrol.[60] It is noteworthy that the present study reveals that $Fe_3O_4$ and $Fe_3O_4$@$SiO_2$ microspheres have high electrical storage density which can be beneficially utilized in developing of electrical energy storage devices and thus pointing towards a novel application possibility of the system. However, since the $Fe_3O_4$@$SiO_2$ microspheres exhibit nearly rectangular cyclic voltagram in the entire frequency range of measurement it will give better performance as EDLC.

## Conclusion

In this work, we have successfully synthesized monodisperse solid $Fe_3O_4$ microspheres (S1) and $Fe_3O_4$@$SiO_2$ core-shell microspheres (S2), respectively, through hydrothermal and a

modified Stöber sol-gel processes and systematically characterized them by PXRD, electron microscopy (FESEM and HRTEM), spectroscopic techniques (FTIR, Raman, UV-Vis and PL spectroscopy), dc magnetic measurements, Mössbauer spectroscopy and cyclic voltammetry. Both S1 and the crystalline core of S2 have cubic spinel structure of $Fd\bar{3}m$ symmetry and each asymmetric unit of S1 and the $Fe_3O_4$ core of S2 have one iron ion vacancy at [B] site. By the Rietveld refinement of PXRD patterns of S1 and S2 we have shown that the crystal lattice gets contracted, microstrain increases, bond angle and bond length change appreciably with incorporation of $SiO_2$ shell on $Fe_3O_4$ microspheres. The dc magnetic and the Mössbauer spectroscopic studies indicate that at 300 K, both the samples are ferrimagnetic in nature but the magnetic properties of $Fe_3O_4$ microspheres change drastically upon surface modification. The values of $H_C$ and hyperfine field reduce substantially upon $SiO_2$ coating on the surface of $Fe_3O_4$ microspheres due to reduction of anisotropy energy. The coercivity and saturation magnetization of $Fe_3O_4$ and $Fe_3O_4$@$SiO_2$ microspheres mainly depend upon the morphology, the synthesis procedure and the average particle size of the individual $Fe_3O_4$ nanoparticle forming the ensemble while the blocking temperature of such system is mainly determined by the inter particle interaction. The cyclic voltagram of S1 shows clear redox peaks at low scan rate (< 0.04 V/s) and these peaks disappear above the scan rate of 0.04 V/s. On the other hand, nearly rectangular shaped cyclic voltagrams are obtained for S2 over the entire range of scan rate. The cyclic voltammetric study suggests that both S1 and S2 can be utilized in fabrication of electrical double layer capacitor.

## Acknowledgement

One of the authors (S.M.) gratefully acknowledges UGC, Govt. of India for providing research fellowship. The PURSE and FIST programs of DST, Govt. of India, UPE program of UGC, Govt. of India and CSIR, Govt. of India (grant number 60(0106)/13-EMR-II) are also acknowledged. We also gratefully acknowledge Prof. R. N. Joardar (Retd.) for helpful discussion.

## Reference

1. Y. S. Lin, S. H. Wu, Y. Hung, Y. H. Chou, C. Chang, M. L. Lin, C. P. Tsai and C. Y. Mou, *Chem. Mater.*, 2006, **18**, 5170.

2. D. Zhang, Z. Liu, S. Han, C. Li, B. Lei, M. P. Stewart, J. M. Tour and C. Zhou, *Nano Lett.*, 2004, **4**, 2151.

3. Z. Liu, D. Zhang, S. Han, C. Li, B. Lei, W. Lu, J. Fang and C. Zhou, *J. Am. Chem. Soc.*, 2005, **127**, 6.

4. Y. Xiong, J. Ye, X. Gu and Q. W. Chen, *J. Phys. Chem. C*, 2007, **111**, 6998.

5. H. Deng, X. Li, Q. Peng, X. Wang, J. Chen and Y. Li, *Angew. Chem. Int. Ed.*, 2005, **44**, 2782.

6. Y. Wang, Q. Zhu and L. Tao, *CrystEngComm*, 2011, **13**, 4652.

7. S. Banerjee, S. O. Raja, M. Sardar, N. Gayathri, B. Ghosh, and A. Dasgupta, *J. Appl. Phys.*, 2011, **109**,123902.

8. S. W. Cao and Y. J. Zhu, *J. Phys. Chem. C*, 2008, **112**, 12149.

9. F. Caruso, M. Spasova, A. Susha, M. Giersig and R. A. Caruso, *Chem. Mater.*, 2001, **13**, 109.

10. X. Liu, Q. Hu, Z. Fang, Q. Wu and Q. Xie, *Langmuir*, 2009, **25**, 7244.

11. D. Yu, X. Sun, J. Zou, Z. Wang, F. Wang, and K. Tang, 2006, **110**, 21667.

12. S. Giri, B. G. Trewyn, M. P. Stellmaker and V. S. Y. Lin, *Angew. Chem. Int. Ed.*, 2005, **44**, 5038.

13. A. Mukhopadhyay, N. Joshi, K. Chattopadhyay, G. De, *ACS Appl. Mater. Interfaces*, 2012, **4**, 142

14. Y. Deng, D. Qi, C. Deng, X. Zhang and D. Zhao, *J. Am. Chem. Soc.*, 2008, **130**, 28.

15. Y. Cheng, R.Tan, W. Wang, Y. Go, P. Cui and W. Song, *J Mater Sci*, 2010, **45**, 5347.

16. X. Xu, C. Deng, M.Gao, W. Yu, P. Yang and X. Zhang, *Adv. Mater.*, 2006, **18**, 3289.

17. B. Luo, X. J. Song, F. Zhang, A. Xia, W. L. Yang, J. H. Hu and C. C. Wang, *Langmuir*, 2010, **26(3**), 1674.

18. M. M. Shirolkar, R. Das, T. Maity, P. Poddar and S. Kulkarni, *J. Phys. Chem. C*, 2012, **116**, 19503.

19. H-J. Zhang, H-M. Xiong, Q-G. Ren, Y-Y. Xia and J-L. Kong, *J. Mater. Chem.,* 2012, **22**, 13159.

20. W. Wang, Z. Li, B. Gu, Z. Zhang and H. Xu, *ACS Nano*, 2009, **3**, 3493.

21. T. Ung, L. M. Liz-Marzán and P. Mulvaney, *J. Phys. Chem. B*, 2001, **105**, 3441.

22. Y. L. Liu, J. L. Zhang, G. Cheng, G. Y. Hong, J. Z. Ni, *Nanotechnology*, 2012, **23**, 425702.

23. G. F. Goya, T. S. Berquo, F. C. Fonseca, M. P. Morales, *J. Appl. Phys.*, 2003, **94**, 3520.

24. C. R. Lin, R. K. Chiang, J. S. Wang and T. W. Sung, *J. Appl. Phys.*, 2006, **99**, 08N710.

25. Y. Zhu, W. Zhao, H. Chen and J. Shi, *J. Phys. Chem. C*, 2007, **111**, 5281.

26. L. P. Zhu, H. M. Xiao, W. D. Zhang, G. Yang, S. Y. Fu, *Cryst. Growth Des.*, 2008, **8**, 957.

27. S. Larumbe, C. Gómez-Polo, J. I. Pérez-Landazábal and J. M. Pastor, *J. Phys.: Condens. Matter,* 2012, **24**, 266007.

28. P. E. Werner, L. Eriksson, and M. J. Westdahl, *J. Appl. Crystallogr.*, 1985, **18**, 367.

29. A. Boultif and D. Louer, *J. Appl. Crystallogr.*, 2004, **37,** 724.

30. A. Altomare, R. Caliandro, M. Camalli, C. Cuocci, C. Giacovazzo, A. G. Moliterni and R. Rizzi, *J. Appl. Crystallogr.*, 2004, **37**, 1025.

31. S. Dey, S. K. Dey, B. Ghosh, V. R. Reddy and S. Kumar, *Mater Chem Phys*, 2013, **138**, 833.

32. S. Dey, S. K. Dey, B. Ghosh, P. Dasgupta, A. Poddar, V. R. Reddy and S. Kumar, *J. Appl. Phys.*, 2013, **114**, 093901.

33. S. Dey, S. K. Dey, S. Majumder, A. Poddar, P. Dasgupta, S. Banerjee and S. Kumar, *Physica B*, 2014, **448**, 247.

34. S. Dey, S. K. Dey, K. Bagani, S. Majumder, A. Roychowdhury, S. Banerjee, V. R. Reddy, D. Das and S. Kumar, *Appl. Phys. Lett.*, 2014, **105**, 063110.

35. L. Lutterotti, MAUDWEB, version 1.9992, 2004, see http://www.ing.unitn.it/~luttero/maud.

36. A. C. Larson and R. B. Von Dreele, "General structure analysis system (GSAS)," Los Alamos National Laboratory, Report LAUR, 86-748, 2000.

37. B. H. Toby, *J. Appl. Crystallogr.*, 2001, **34**, 210.

38. J. Sun, G. Yu, L. Liu, Z. Li, Q. Kan, Q. Huob and J. Guan, *Catal. Sci. Technol.*, 2014, **4**, 1246.

39. G.H. Du, Z.L. Liu, X. Xia, Q. Chu and S.M. Zhang, *J Sol-Gel Sci Techn*, 2006, **39**, 285.

40. A. Roychowdhury, S. P. Pati, S. Kumar and D. Das, *Powder Technol.*, 2014, **254**, 583.

41. M. Gao, W. Li, J. Dong, Z. Zhang and B. Yang, *World J. Condens. Matter Phys.*, 2011, **1**, 49.

42. L. B.-Gurlet, D. Neff, S. Réguer, J. Monnier, M. Saheb and P. Dillmann, J. Nano. Res., 2009, **8**, 147.

43. D. L. A. De Faria, S. V. Silva and M. T. D. Oliveira, *J. Raman Spectrosc.*, 1997, **28**, 873.

44. P. Peikertová, M. Vaculíc, P. Filip and J. Kukutschová, Proceeding of the 4th International Conference NANOCON, Brno, Czech Republic, 2012.

45. N. Maxim, A. Overweg, P. J. Kooyman, J. H. M. C. van Wolput, R. W. J. M. Hanssen, R. A. van Santen and C. L. Abbenhuis, *J. Phys. Chem. B*, **2002**, 106, 2203.

46. C. Hui, C. Shen, J. Tian, L. Bao, H. Ding, C. Li, Y. Tian, X. Shiab and H. J. Gao, *Nanoscale*, 2011, **3**, 701.

47. K. Lagarec and D. G. Rancourt, Recoil-Mössbauer Spectral Analysis Software for Windows (University of Ottawa Press, Ottawa, 1998).

48. T. J. Daou, G. Pourroy, J. M. Greneche, A. Bertin, D. F. Flescha and S. B. Colin, *Dalton Trans.*, 2009, **23**, 4442.

49. B. Y. Yu and S. Y. Kwak, *J. Mater. Chem.*, 2010, **20**, 8320.

50. Y. Cheng, B. Zou, C. Wang, Y. Liu, X. Fan, L. Zhu, Y. Wang, H. Maa and X. Cao, *CrystEngComm*, 2011, **13**, 2863.

51. H. Sun, B. Chen, X. Jiao, Z. Jiang, Z. Qin and D. Chen, *J. Phys. Chem. C*, 2012, **116**, 5476.

52. J. Lee, S. Yoon, T. Hyeon, S. M. Oha and K. B. Kimb, *Chem. Commun.*, 1999, **21**, 2177.

53. J. Kim, J. E. Lee, J. Lee, J. H. Yu, B. C. Kim, K. An, Y. Hwang, C-H. Shin, J-G. Park, J. Kim and T. Hyeon, *J. Am. Chem. Soc.*, 2006, **128**, 688.

54. W. Zhao, J. Gu, L. Zhang, H. Chen and J. Shi, *J. Am. Chem. Soc.*, 2005, **127**, 8916.

55. F. Tian, G. Chen, P. Yi, J. Zhang, A. Li, J. Zhang, L. Zheng, Z. Deng, Q. Shi, R. Peng and Q. Wang, *Biomaterials*, 2014, **35**, 6412.

56. H. Chen, C. Deng and X. Zhang, *Angew. Chem. Int. Ed.*, 2010, **49**, 607.

57. B. Lv, Y. Xu, H. Tian, D.Wu and Y. Sun, *J. Solid State Chem*., 2010, **183**, 2968.

58. P. Zhao, Y. Zhu, X. Yang, J. Shen, X. Jiang, J. Zong and C. Li, *Dalton Trans.*, 2014, **43**, 451.

59. G. Bai, X. Lan, X. Liu, C. Liu, L. Shi, Q. Chen and G. Chen, Green Chem., 2014, **16**, 3160.

60. G. Bai, L. Shi, Z. Zhao, Y. Wang, M. Qiu and H. Dong, Mater. Lett., 2013, **96**, 93.

**Figure Caption**

**Fig.1** The final Rietveld plot (output file of GSAS) of (a) S1 and (b) S2, showing the difference (pink color line) between the experimental (red color symbol) and the simulated pattern (green color line).

**Fig.2** Unit cell of (a) S1 and (b) S2 showing the tetrahedral (A) and octahedral [B] sites, along with the bond angles and lengths.

**Fig.3** (a), (b) and (c) FESEM micrograph, (d) EDS spectrum of S1.

**Fig.4** (a), (b) and (c) FESEM micrograph, (d) EDS spectrum of S2.

**Fig.5** HRTEM micrograph of S1 showing (a) and (b) $Fe_3O_4$ microspheres, (c) $Fe_3O_4$ nanoparticle and (d) SAED pattern of S1.

**Fig.6** HRTEM micrographs of S2 showing $Fe_3O_4$@$SiO_2$ core-shell microspheres.

**Fig.7** FTIR spectra of S1 and S2.

**Fig. 8** Raman spectra of S1 and S2. # and * indicate the peaks for $Fe_3O_4$ and $SiO_2$, respectively.

**Fig.9** Schematic representation of the formation of $Fe_3O_4$@$SiO_2$ core-shell structure. The $Fe_3O_4$ core is shown at the center.

**Fig. 10** UV-Vis absorption spectra of S1 and S2.

**Fig.11** Photoluminescence (PL) emission spectra of S1 and S2.

**Fig.12** Mössbauer spectra of (a) S1 and (b) S2 fitted by the "Lorentzian site analysis" of the Recoil program.

**Fig.13** ZFC-FC magnetization of (a) S1 and (b) S2 at 100 Oe external magnetic field.

**Fig.14** M-H (hysteresis) loops of S1 and S2 at 300, 100 and 5 K (shown between ±0.2 T for clarity).

**Fig.15** Cyclic voltagram (CV) of (a) ITO-S1 film and (b) ITO-S2 film at different scan rate.

**Table Caption**

**Table 1** Crystal Data and Refinement parameters obtained by MAUD[†] and GSAS[*] programs

**Table 2** Bond distances and bond angles obtained by GSAS program

**Table 3** Values of room temperature Mössbauer parameters of S1 and S2 determined by Lorentzian site analysis of Recoil program [IS=Isomer shift, QS= Quadrupole shift, HMF=hyperfine magnetic field, (A)=tetrahedral site, [B]=octahedral site, [S]=disordered surface region]

**Table 4** Values of saturation magnetization ($M_{SAT}$) and Coercivity ($H_C$) at different temperature obtained from the M-H (hysteresis) loop measurement

**Table 1** Crystal Data and Refinement parameters obtained by MAUD[†] and GSAS[*] programs

| Parameters | $Fe_3O_4$ (S1) | $Fe_3O_4$@$SiO_2$ (S2) |
|---|---|---|
| Formula[†,*] | $Fe_{2.9}O_4$ | $Fe_{2.9}O_4$ |
| Formula Weight[†,*] | 231.55 | 231.55 |
| Crystal System[†,*] | Cubic | Cubic |
| Space group[†,*] | Fd-3m | Fd-3m |
| Crystallite size (nm)[†] | 46.7 | 26.3 |
| Microstrain ($\times 10^{-4}$)[†] | 7.72 | 27.77 |
| a (Å)[*] | 8.37685(6) | 8.34198(10) |
| V [$Å^3$][*] | 587.82(1) | 580.51(1) |
| Position of O atom* | 0.2549 | 0.2598 |
| Z[*] | 8 | 8 |
| $D_{cal}$/ $gcm^{-3}$* | 5.233 | 5.299 |
| $\mu_{CuK\alpha}/mm^{-1}$* | 115.976 | 117.436 |
| $R_{wp}$[†] | 0.066 | 0.015 |
| $R_{exp}$[†] | 0.041 | 0.089 |
| GOF | 1.64 | 1.66 |
| $R_{wp}$[*] | 1.57 | 2.23 |
| $R_p$[*] | 0.94 | 1.44 |
| $R_F^2$* | 2.40 | 3.15 |
| $\chi^2$* | 1.96 | 1.13 |

**Table 2** Bond distances and bond angles obtained by GSAS program

| Sample | Bond Distance (Å) | | Bond Angle (°) | |
|---|---|---|---|---|
| | A−O | B−O | O−A−O | O−B−O |
| S1 | 2.045(1) | 1.900(1) | 109.5(1) | 87.7(1) |
| | | | | 93.3(2) |
| S2 | 2.073(2) | 1.944(2) | 109.5(2) | 85.2(2) |
| | | | | 94.8(4) |

**Table 3** Values of room temperature Mössbauer parameters of S1 and S2 determined by Lorentzian site analysis of Recoil program [IS=Isomer shift, QS= Quadrupole shift, HMF=hyperfine magnetic field, (A)=tetrahedral site, [B]=octahedral site, [S]=disordered surface region]

| Sample | Site | IS (±0.03) (mm $s^{-1}$) | QS (±0.03) (mm $s^{-1}$) | HMF (±0.4) (T) | Width (±0.03) (mm $s^{-1}$) | Area (±0.2) (%) |
|---|---|---|---|---|---|---|
| S1 | (A) | 0.56 | 0.11 | 56.2 | 0.45 | 46.8 |
| | [B] | 0.78 | 0.25 | 49.1 | 0.43 | 53.2 |
| S2 | (A) | 0.40 | 0.22 | 55.0 | 0.42 | 38.1 |
| | [B] | 0.81 | 0.31 | 48.3 | 0.36 | 50.8 |
| | [S] | 0.33 | -0.21 | 47.2 | 0.31 | 11.1 |

**Table 4** Values of saturation magnetization ($M_{SAT}$) and Coercivity ($H_C$) at different temperature obtained from the M-H (hysteresis) loop measurement

| Sample | Temperature (K) | $M_{SAT}$ (emu $g^{-1}$) | $H_C$ (Oe) |
|---|---|---|---|
| S1 | 300 | 63.5 | 200 |
| | 100 | 69.4 | 500 |
| | 5 | 70.0 | 900 |
| S2 | 300 | 38.5 | 120 |
| | 100 | 43.0 | 300 |
| | 5 | 44.1 | 550 |

## Table of content

# A comparative study on structural, optical and magnetic properties of $Fe_3O_4$ and $Fe_3O_4@SiO_2$ core-shell microspheres along with assessment of their potentiality as electrochemical double layer capacitor

S. Majumder,[a, b] S. Dey,[a] K. Bagani,[b] S. K. Dey,[a] S. Banerjee[b,*] and S. Kumar[a,*]

[a] Department of Physics, Jadavpur University, Kolkata – 700032, India

[b] Saha Institute of Nuclear Physics , 1/AF Bidhannagar, Kolkata – 700064, India

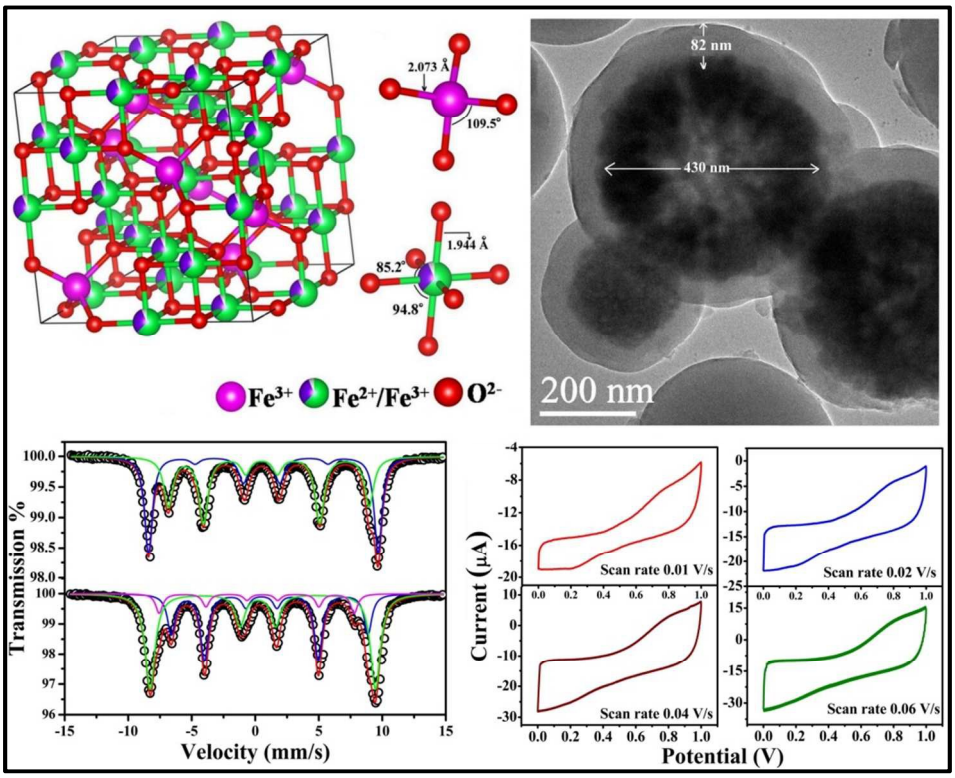


The magnetic and hyperfine properties of $Fe_3O_4$ and $Fe_3O_4@SiO_2$ microspheres depend on synthesis procedure, morphology, surface property, the collective properties of the nanoparticle assembly and the average size of individual nanoparticle forming the spherical ensemble, but not on the diameter of the microspheres. $Fe_3O_4@SiO_2$ can be used for fabrication of electrical double layer capacitor.